Available online at www.sciencedirect.com

ScienceDirect

Solid Earth Sciences 10 (2025) 100262

www.elsevier.com/locate/SESCI

Impact of extremely low porosity on geothermal gradient and fluid migration in gas hydrate-bearing layers: A case study of South Shetland Islands, Antarctic Peninsula

Doğa Düşünür Doğan [a,*], Selvican Türkdoğan [a,b,c], Neslihan Ocakoğlu [a], Umberta Tinivella [d], Michela Giustiniani [d], Zehra Altan [a], Sinan Arık [a]

[a] Department of Geophysical Engineering, Istanbul Technical University, Maslak, 34469, Istanbul, Turkey
[b] Department of Engineering Geology and Hydrogeology, RWTH Aachen, 52064, Aachen, Germany
[c] Department of Earth Sciences, Institute of Geophysics, Seismology and Geodynamics, ETH Zürich, 8092, Zürich, Switzerland
[d] Istituto Nazionale di Oceanografia e di Geofisica Sperimentale - OGS, 34010, Sgonico, Italy

Received 14 February 2025; revised 11 August 2025; accepted 11 August 2025
Available online 28 August 2025

Abstract

Numerical fluid flow models were employed for the first time to study gas hydrates in South Shetland Islands, Antarctic Peninsula. The complexity of its geology, added to the remote and environmentally sensitive characteristics, makes it a very unique natural laboratory, where studying processes that could influence gas hydrate stabilityremains highly challenging. Based on seismic data, a marine subsurface model was created and fluid flow simulations carried out with ANSYS Fluent. Key inputs like sediment thickness, in-situ faults, and fractures, and water column dimensions were obtained from seismic sections. The same value of thermal and physical rock properties was assumed for each geological unit; the mesh structure was developed using triangular discretization. Four numerical models were constructed to investigate how variations in porosity, particularly under extremely low-porosity conditions, might affect thermal and fluid flow behavior within hydrate-bearing sediments. Porosity values of 0.01, 0.05, 0.1, and 0.2 were systematically applied to represent the low-porosity regimes. The results highlight that, especially at extremely low porosity, porosity together with fault density and seafloor bathymetry can strongly shape the distribution of heat transfer and fluid migration patterns. While the models do not directly simulate gas hydrate dissolution, the findings suggest that localized thermal anomalies and structural complexities could potentially create conditions favorable to destabilization processes. These insights contribute to a better understanding of the geophysical and hydrodynamic factors that may influence gas hydrate systems in complex and sensitive geological settings.

Keywords: Gas hydrate; Numerical modelling; Antarctica; Multichannel seismic; Porosity

1. Introduction

Gas hydrates are crystalline structures that under specified conditions of low temperature and high pressure, in marine and permafrost regions, form from the entrapment of gas molecules, especially methane, into lattices of water molecules. In this view, they represent a possible energy resource and an important component of the global carbon cycle (Kvenvolden, 1998, 2002). With respect to these systems, porosity and permeability are among the many key factors in determining their behavior and dynamics. These properties govern the fluid migration, heat transfer, and general stability of the hydrate bearing sedimentary layers, issues that have important implications to methane release, energy extraction, and geohazard risk.

According to Aharonov et al. (1997), permeability reduction in sediments may either be due to reduced porosity or due to

* Corresponding author.
E-mail addresses: dusunur@itu.edu.tr (D.D. Doğan), turkdogans@itu.edu.tr (S. Türkdoğan), neslihan@itu.edu.tr (N. Ocakoğlu), utinivella@ogs.it (U. Tinivella), mgiustiniani@inogs.it (M. Giustiniani), zaltan@itu.edu.tr (Z. Altan), ariks@itu.edu.tr (S. Arık).

https://doi.org/10.1016/j.sesci.2025.100262

constricted pathways of migration without any change in porosity. In systems containing hydrates, the permeability usually decreases as a function of direct reduction in porosity due to hydrate accumulation, which plugs the sediment pores and fractures (Nimblett and Ruppel, 2003). This behavior is even more significant in low-porosity layers, where the interaction between gas hydrate formation, fluid flow, and thermal dynamics is stronger. For example, fractures tend to clog before the porous medium in sediments with pore diameters or fracture apertures greater than 1 mm. Moreover, data from the Blake Ridge presents case study of such systems with juxtaposed fractured and porous sediments. Downhole data from this area demonstrate that gas hydrate concentrations increase with depth and may fill up to 10–15 % of pore space in the deeper portions (Lee, 2000). Increasing hydrate saturation thus stiffens the sediment aggregate (Durham et al., 2003), modifies bulk moduli, and increases seismic velocities (Ecker et al., 1998; Helgerud et al., 1999). These effects reflect both hydrate accumulation and sediment compaction, as porosity decreases from ~70 % at the seafloor to ~55 % near the bottom simulating reflector (Paull et al., 1996). A review of published field and logging studies indicates that porosities measured in many well-documented marine gas-hydrate occurrences are typically in the tens of percent rather than at the single-percent level (e.g., Blake Ridge, Nankai and Gulf of Mexico sites). While compacted or lithified fine-grained rocks at greater burial depths can exhibit much lower porosities, such lithified units are not commonly reported as the primary host for extensive hydrate accumulations within the gas-hydrate stability zone (GHSZ). For this reason we treat the porosity = 0.01 model in this study as an extreme sensitivity case that explores the thermal and hydrodynamic response of an unusually low-porosity host; we discuss below how such an end-member informs our understanding of porosity controls even if it is not representative of the bulk of documented hydrate reservoirs. Previous observations indicate that any comprehensive understanding of gas hydrate behavior needs to take both fractured and porous sedimentary systems into consideration.

Sedimentation rates and methane expulsion processes are other parameters that contribute to fluid flow and methane transport in hydrate systems. For example, disequilibrium compaction due to rapid deposition can force pore fluids upward and may lead to the development of hydrate layers that have high concentrations of methane (Hyndman and Davis 1992). Additionally, methane recycling at the base of the hydrate zone and thermodynamic equilibrium processes contribute to the observed fluxes of methane towards the seabed. Fractures often dominate flow pathways, facilitating fluid migration while simultaneously sequestering gas due to lower capillary pressures (Bethke et al., 1991). Such complexities necessitate a detailed understanding of the coupling between fluid flow, heat transfer, and sediment structure in hydrate-bearing formations.

Numerical modeling has become essential for investigating gas hydrate processes, offering insights that are difficult to obtain from field data alone. It enables the simulation of complex interactions between porosity, permeability, temperature, and hydrate accumulation, creating a robust framework for understanding how these variables influence one another under varying geological and environmental conditions. This study specifically examines the behavior of low-porosity gas hydrate layers in their interaction with fluid flow and temperature distribution. Such research helps fill knowledge gaps, enhances the prediction of hydrate dynamics, and informs strategies for resource recovery, environmental protection, and geohazard mitigation. The importance of such modeling cannot be overstated, as it improves both theoretical understanding and practical applications in energy extraction and climate change studies. However, alongside the potential of hydrates as an energy source, destabilization of these structures poses significant risks to seabed and infrastructure integrity. Accurate modeling of this process requires consideration of various factors, including regional geology, pressure and temperature fluctuations, and fluid dynamics processes that govern hydrate formation and degradation.

Previous studies have proposed the potential presence of hydrates in Antarctic sediments but have emphasized the need for further studies to understand distribution, stability, and potential consequences for the environment. The present work proposes a finite volume numerical model for simulation of hydrate behavior in Antarctic Peninsula and South Shetland Islands' subsurface marine sediments for the first time ever. ANSYS Fluent is utilized in this work for developing a high-fidelity earth model with real-time simulation capabilities. For the first time, in this work, temperature, pressure, and velocity fluctuations in hydrate-bearing sediments during hydrate dissociation have been analyzed, and in addition, an investigation of active tectonic processes, such as faulting and seabed topography, and its impact on hydrate stability and behavior during dissociation have been conducted.

1.1. Study area and gas hydrate occurrence

The South Shetland Continental Margin, located off the Antarctic Peninsula, is both tectonically active and geologically complex (Fig. 1a). Key tectonic elements include the subduction of the South Sandwich Plate beneath the South American Plate and the opening of the Drake Passage. The present subduction is oceanic plate sinking and roll-back, accompanied by extension in the Bransfield Strait marginal basin (Larter and Barker, 1991; Kim et al., 1995; Dietrich et al., 2004). This margin is bounded by four major structures: the Shackleton Fracture Zone (SFZ) to the northeast, the Hero Fracture Zone (HFZ) to the southwest, the South Shetland Trench (SST) to the northwest, and the Bransfield Strait (BS) to the southeast (Fig. 1a). The SFZ is still tectonically active while the HFZ is inactive because of the cessation of the ridge spreading. Barker (1982); Barker and Dalziel (1983). These fracture zones define the Bransfield microplate, which, as a fact, is surrounded by high seismicity, concentrated mainly around submarine volcanoes and/or rifted regions (Tinivella et al., 2008; Dziak et al., 2015).

Seismic analyses, including Common Image Gather (CIGs) and Prestack Depth Migration (PSDM), found evidence of

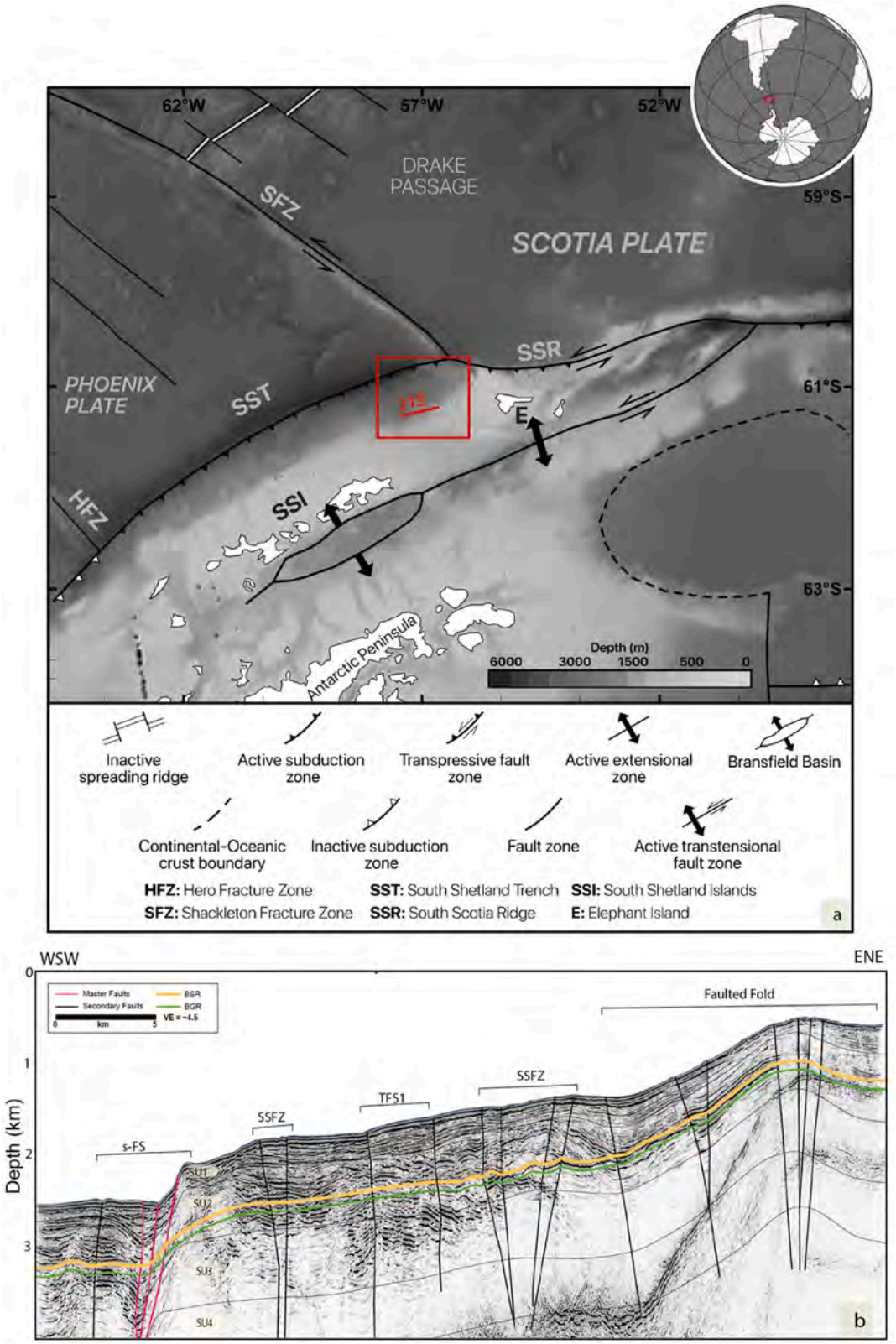

Fig. 1. **a** Tectonic framework of the Scotia Arc (modified from Zaldivar et al., 2006, and references therein). DEM of the study area was produced by GEBCO Bathymetry Data and Natural Earth Data (http://www.gebco.net/). **b** Reinterpreted pre-stack depth migrated (PreSDM) seismic section of Profile 213 Loreto et al. (2011). BSR and Bottom of Gas Reflector (BGR) are traced by yellow and green color respectively. TFS1: Transcurrent Fault System, SSFZ: Strike-slip Fault Zone, SU: Seismic Unit. Vertical exaggeration 1:4.

important gas hydrates in this area. The BSR suggests that there is free gas underneath the hydrate layer within a structurally complex sedimentary prism (Tinivella et al., 2009; Tinivella, 1999; Tinivella, 2002; Tinivella et al., 1998; Tinivella et al., 2002; Song et al., 2018; Lodolo et al., 2002). Gravity core studies confirm the presence of free gas and a base gas reflector in the area (Tinivella et al., 2008). Because it was of shallow depth relative to that in the south, the BSR is decoupled from the Opal A/CT transition (Neagu et al., 2009; Jin et al., 2003). Gas hydrate and free gas systems depend on geological factors in such an actively tectonic zone, but rather regional hydrate stability zone and associated gases characterization is demanded by Loreto and Tinivella (2012).

The primary factors contributing to this phenomenon are the uneven distribution of subsurface fluids, heat flow instability, evolving geological settings influenced by surface processes in the lithosphere, and the extreme pressure conditions of pore fluids at depth. Solovyov et al. (2011) suggested that the active tectonism in the Antarctic continental block, such as fissure formations or geodynamic disturbances, might be connected with oil and gas sedimentation. This system of subglacial drainage fosters the migration of fluids and gases through the lithosphere towards the Antarctic continental margin, creating a reservoir of hydrocarbons. It is further evidenced by the astonishing thickness of the free gas layer, attested to reach 300 m locally according to Tinivella et al. (2009), which could evidence deep gas feeding, as modelled by Vargas-Cordero et al. (2021).

1.2. Seismic data

The seismic data used in this study were collected during two separate surveys conducted in the 1989/90 and 1996/97 Austral summers aboard the R/V OGS Explora as part of the Italian National Antarctic Program (PNRA). The same datasets have been previously processed and interpreted by Tinivella et al. (2009) and Loreto et al. (2011). They produced PreSDM sections and derived 2-D velocity fields by iterative pre-stack depth migration using the Kirchhoff algorithm within Seismic Unix software and codes developed in-house. The estimate for the volume of gas hydrate varied between 16×10^9 and 20×10^9 m^3, according to Loreto et al. (2011), whereas the volume of free gas within this interval was estimated to range from 1.68 to 2.8×10^{12} m^3, based on seismic velocity data with a modified Biot-Geerstma-Smit theory. The BSRs were mapped as gas hydrates in a number of seismic profiles, and Profile 213 has continuous BSR along the seafloor topography in the area of velocity lateral variation (Fig. 1b).

Seismic data in this present study are analyzed using the commercial software Echos AspenTech, and the PreSDM section has been reinterpreted down to approximately 4.0–5.0 km depth. The sea floor is pretty rough, based on topographic faults, folds, and canyons. Seismic strata are very deformed due to active faults. These deformation zones are identified as shear zones, in which faults do not result in significant thickness changes in the overall strata but still produce vertical displacement of the seafloor and subfloor sediments. High-angle faults are interpreted to be strike-slip fault zones that develop flower structures in some places while converging at depth. One of the main faults, mapped for long distances using bathymetric data, was firstly interpreted by Loreto et al. (2011) as a left-lateral transcurrent system with a normal component (TFS1). This fault system shows two E–W trending segments, whose northern continuation is also imaged in Profile 213. Moreover, a secondary fault system (s-FS) shows a normal movement with a vertical offset of about 500 m, which contributes to basin development (Fig. 1b). Seismic profiles and velocity models stratigraphically are the important keys for understanding the geological feature in this area. Seismic units are defined according to their reflection characteristics and velocity distribution. The seismic section consists of six main units, each with distinct characteristics. SU1, the most superficial unit, is composed of recent sediments with parallel reflections and velocities ranging from 1400 to 1700 m/s. SU2 and SU3 are characterized by chaotic and weak reflections, with the base of SU2 aligning with the Bottom Simulating Reflector (BSR) and extending up to 100 m below it. Significant lateral velocity variations appear in SU2. In general, velocity anomalies above the BSR range between 100 and 200 m/s. In contrast, the deeper units, SU4, SU5, and SU6, exhibit high average velocities exceeding 3500 m/s. This interpretation of the seismic section serves as the foundation for the model geometry discussed in the following sections.

1.3. Numerical modeling

Numerical modeling of gas hydrates in Antarctica requires an integration of knowledge in geology, physics, chemistry, and mathematics. These models provide the necessary information on how gas hydrates of this remote region will act and support decisions related to environmental management. The common methods-usually finite element or finite difference-solve equations governing heat transport, fluid flow, and chemical reactions by subdividing the area of interest into small computational cells. Such computational techniques represent complex dynamics of the gas hydrates while enabling researchers to study their interactions and implications for environmental science. This work has applied a finite volume-based numerical simulation that includes factors such as sediment thickness, faults, bathymetric variations, pressure-temperature conditions, and sediment porosity. The details of the modeling process are given in the following sections.

To simulate the fluid flow dynamics in the selected 2D seismic profile (213), this study has utilized a coupled transient numerical solution and heat transport approach. The finite volume-based Computational Fluid Dynamics (CFD) software, ANSYS FLUENT (ANSYS, 2018), is employed to obtain the numerical solution of the steady-state Navier–Stokes equations (e.g., Patankar, 1980; Holmes and Connell, 1989). The fluid flow is modeled as laminar and viscous, with inertial effects neglected due to very slow accelerations. Darcy's law governs the flow, and fluid density is assumed to vary with temperature according to the Boussinesq approximation (Fontaine and

Wilcock, 2007; Düşünür Doğan and Üner, 2019; Üner et al., 2019; Loreto et al., 2019; Üner and Dusunur Dogan, 2021). The porous media are assumed to be in local thermal equilibrium, meaning that the fluid temperature within the pores is equal to the solid temperature at the same location.

The geometry of the model was realized by using ANSYS Design Modeler, with particular attention to geological features like fault geometry and sediment thickness, derived from depth-migrated seismic sections by Loreto et al. (2011) and integrated into the seismo-stratigraphic units to build a strong subsurface representation (Fig. 2a). This model has a domain size of about 42 km wide and 4.6 km deep, covering the essential geological and physical parameters of the region. The model was then discretized into triangular elements, interconnected at 96,191 nodes for an accurate numerical representation, as shown in Fig. 2b. It was decided after a series of tests that the mesh was optimal in size and was made with a minimum size of 10 m near the faults to resolve areas critical in fluid flow and thermal analysis. In contrast, the bedrock utilized coarser mesh elements of up to 100 m in size, ensuring computational efficiency and a high enough resolution to resolve the thermal and flow regimes accurately. he quality of the generated mesh is assessed based on skewness and overall mesh quality criteria, ensuring its suitability for accurate numerical simulations. For triangular and tetrahedral meshes in most flow applications, it is recommended that the maximum skewness remains below 0.95, with an average skewness value of less than 0.33, to minimize numerical errors and enhance solution accuracy (Fig. 2c). Additionally, the overall mesh quality should exceed 0.90 to ensure optimal element distribution and computational efficiency (Fig. 3d). The mesh employed in this study satisfies these criteria, confirming its adequacy for reliable computational analysis. These refined configurations are going to be a sound basis for the numerical simulations subsequently carried out.

Fault structures were one of the major concerns due to their significant disruption effects on the fluid flow and thermal regimes. The model faults are relatively much more permeable than the host rocks and are assumed to be 50 m thick. Permeability may vary over a wide range, up to two orders of magnitude Fairley and Hinds (2004); Bense and Person (2006), depending on the local thermal and hydraulic setting. This variation reinforces the dual role of faults as conduits or barriers to fluid flow, as suggested by Heffner and Fairley (2006). Surrounding sedimentary units include methane-rich deposits and basaltic bedrock, each of which controls subsurface fluid dynamics. Representative permeability, porosity, and thermal conductivity values for sediments, faults, and the basement are given in Tables 1 and 2. The variation of viscosity with temperature was incorporated by implementing two User Defined Functions (UDFs), which better represents the realistic properties of the fluids at various subsurface environments.

Boundary conditions were implemented with much care in order to realistically represent the physics of the problem. The vertical boundaries were adiabatic and impermeable. It means that any kind of mass and heat transfer through the sidewalls was not allowed and isolated the modelled domain. Horizontal boundaries were assumed to be isothermal. According to Tinivella and Accaino (2000), the temperature of the seabed was set to 2 °C for the upper wall boundary. A temperature gradient of 37.5 °C/km (Loreto et al., 2011) was then applied homogeneously within the model domain to simulate the

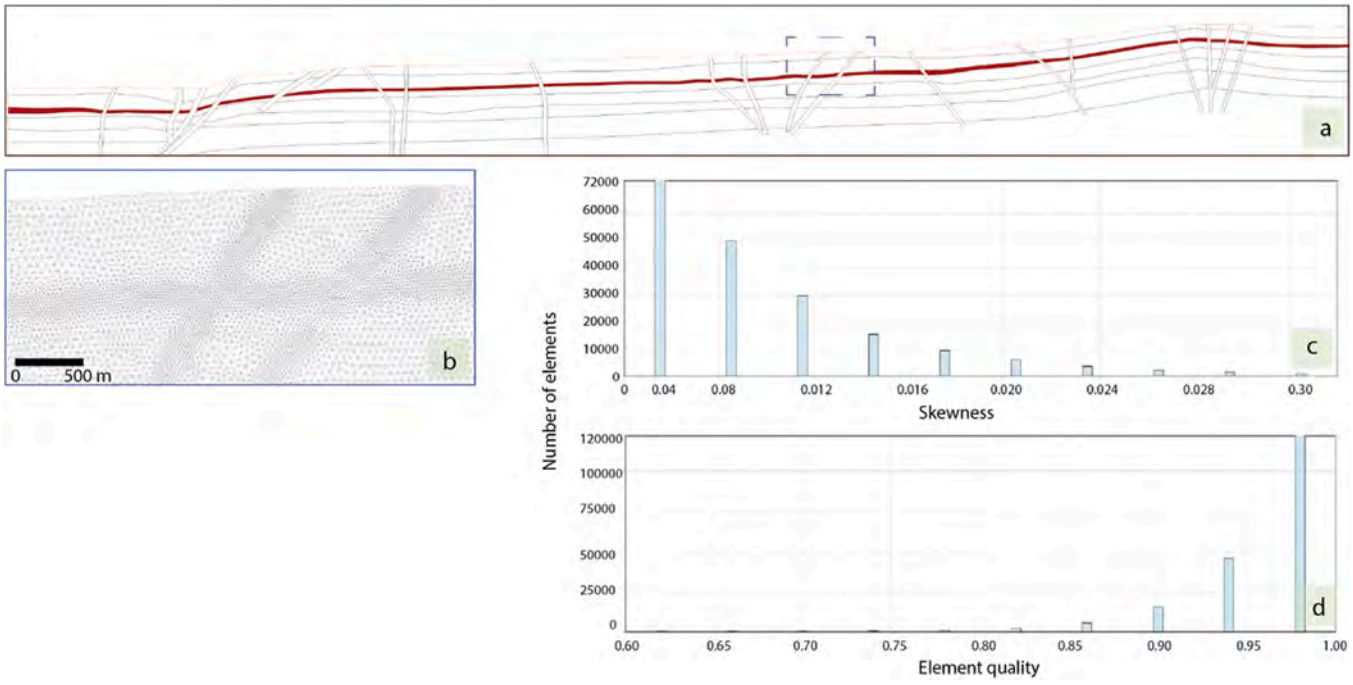

Fig. 2. **a** Model geometry for numerical calculations, **b** The mesh geometry of the area indicated by the square in the model geometry has been magnified and displayed **c** Skewness of the mesh **d** Element quality of the mesh.

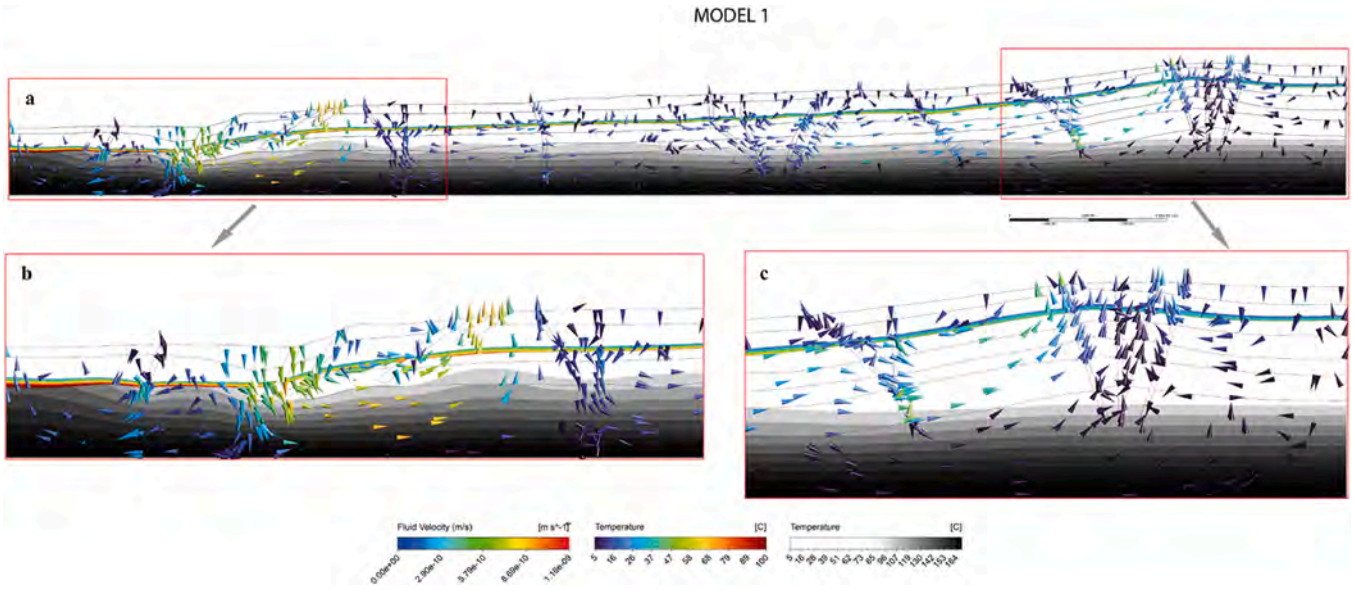

Fig. 3. **a** Temperature distribution overlaid with fluid flow vectors for Model 1. Zoomed-in views of the regions marked with red squares are presented in panels **b** and **c**.

Table 1
Properties of geological units.

Units	Permeability (m^2)	Porosity (1)	Thermal Conductivity (W/mK)
Sedimentary	1.00e-16	0.2	2.5
Fault	1.00e-15	0.1	2.5
Basement	1.00e-17	0.03	2.5

Table 2
Properties of fluid.

Parameter	Value	Unit
Density of fluid (ρ_0)	1000	kg/m^3
Dynamic viscosity of fluid (μ)	$5e^{-5}$	kg/m.s
Specific heat capacity (Cp)	4200	J/kg.K
Thermal expansion coefficient (β)	$2.07e^{-4}$	1/K

thermal structure of the region. Simulations also included differential pressure gradients, due to the undulated seabed topography, which were important for fluid dynamics modeling with accuracy. Interval velocities derived from previous velocity analyses (Loreto et al., 2011) were used to estimate the depth portions in creating a detailed numerical representation of the subsurface. Calculations of water column pressure were made for each segmented portion of the seafloor to accurately model pressure effects throughout the domain. The integrated model thereby captures the effective interaction of geological structures, thermal regimes, and fluid flow dynamics.

In the study, numerical modeling has been carried out to investigate the temperature distribution and fluid flow within and around a gas hydrate-bearing sediment layer, with a particular focus on extremely low-porosity conditions. The present study developed four different numerical models, Models 1–4, for which the porosity was systematically assigned to 0.01, 0.05, 0.1, and 0.2. These values were selected to represent low-porosity regimes, with the lowest values reflecting extreme cases. These simulations have attempted to highlight how changes in porosity—especially under extremely low-porosity conditions—force the system to change its thermal and hydrodynamic behaviors, and most importantly, the interaction of the hydrate layer with the outside world. Interpretation of results for all these models is performed by identifying general trends and controlling mechanisms that may be representative of the role played by porosity, particularly at extremely low values, in determining thermal exchange and fluid migration inside these kinds of geologic structures.

2. Results and discussion

Several fluid flow models have been developed to investigate and understand dispersion and behaviors of various porosity values within gas hydrate layers. These models have been developed to study how changes in porosity might affect fluid flow and heat transfer within the reservoir. Changes in the efficiency of heat transfer, in turn, will also locally affect the distribution of temperatures, which might alter stability conditions for gas hydrate and thus promote their dissociation. Results are presented and analyzed for Models 1–4, where the porosity values were systematically assigned as 0.01, 0.05, 0.1, and 0.2, respectively (Figs. 3–6).

Methane dissolution in marine sediments occurs when methane gas is released from the sub-seafloor and dissolves in pore water present in the sediment. The dissolved methane can then diffuse through the sediment and may be oxidized by microorganisms, which consume methane as an energy source, producing CO_2 and hydrogene as by-products. Alternatively, the methane can accumulate in the sediment, forming gas

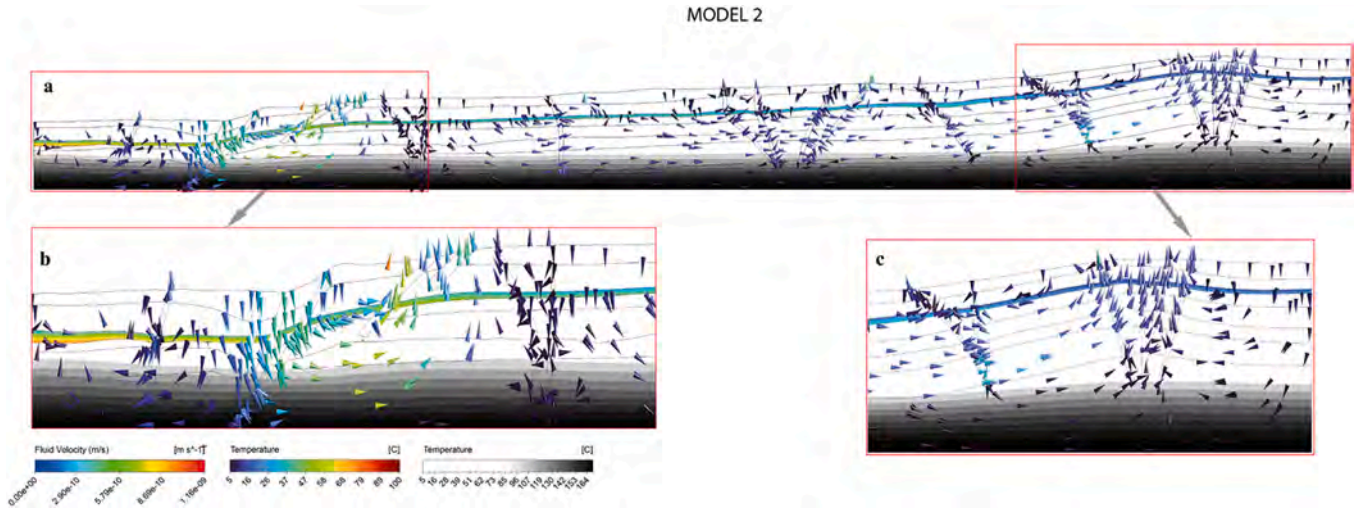

Fig. 4. **a** Temperature distribution overlaid with fluid flow vectors for Model 2. Zoomed-in views of the regions marked with red squares are presented in panels **b** and **c**.

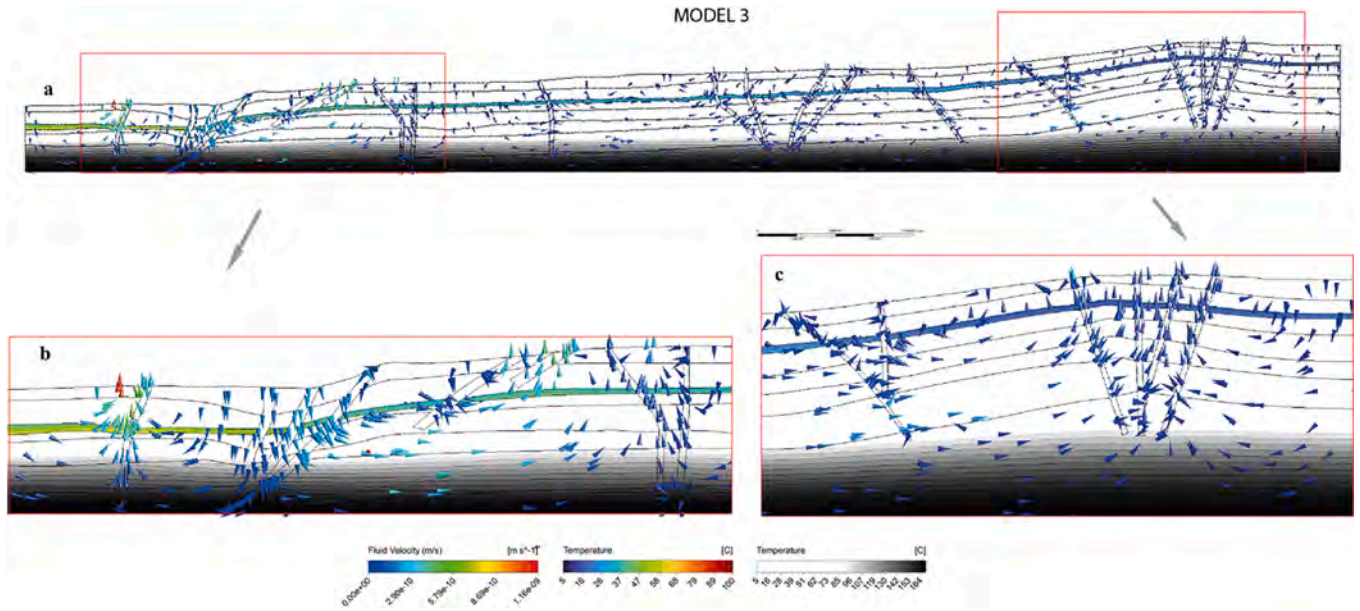

Fig. 5. **a** Temperature distribution overlaid with fluid flow vectors for Model 3. Zoomed-in views of the regions marked with red squares are presented in panels **b** and **c**.

hydrates if the pressure and temperature conditions are suitable. The process of methane dissolution in marine sediments is influenced by various factors, including sediment properties, water depth, temperature, and pressure, as well as the presence of methane-producing organisms and active fault structures.

The methane produced by methanogenesis can then dissolve in the groundwater, forming methane-rich fluids that may accumulate in subsurface sediments. Additionally, the reaction of methane with groundwater in marine sediments can also lead to the formation of methane hydrates. If the concentration of dissolved methane in groundwater is high enough, the methane can combine with water molecules to form methane hydrates, which can accumulate in subsurface sediments or at the seafloor. No source of methane has been specified in our models; hence the simulations do not address issues of the process of gas hydrate formation. The models account instead for a layer of sediments containing gas hydrates outlined in seismic sections, assuming that the fractional amount of gas hydrate in the pore space does not vary with time.

Model simulation for a Model1 where the porosity value is taken as 0.01 is shown in Fig. 3. A BSR level is observed continuously along the seismic line number 213, extending over a distance of more than 30 km. The presence of active in-situ faults significantly impacts fluid flow velocities, resulting in more efficient heat transfer, unlike other parts of the sediment. Previous research has particularly deliberated on the

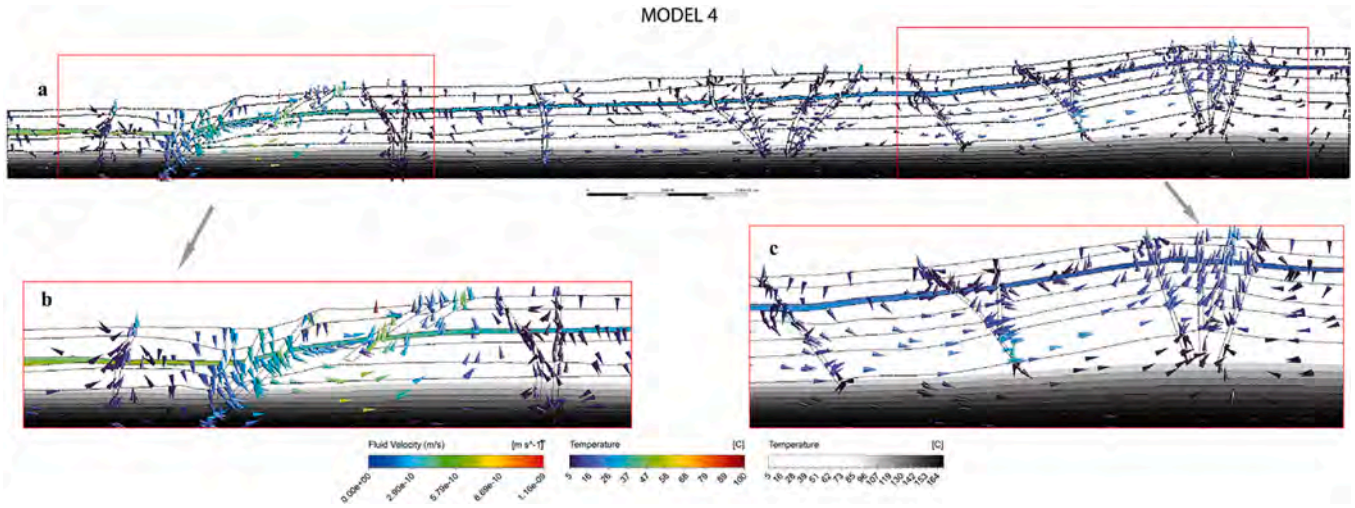

Fig. 6. **a** Temperature distribution overlaid with fluid flow vectors for Model 4. Zoomed-in views of the regions marked with red squares are presented in panels **b** and **c**.

significance of the presence of faults and their impact on fluid flow in marine environment (Loreto et al., 2019; Düşünür-Dogan and Üner, 2019; Şen and Doğan, 2021; Düşünür-Dogan, 2023).

On a large scale, the isotherms generally represent a smooth, continuous distribution across all models. Small-scale variations along model faults do occur. For instance, in places where the fault increases downward fluid migration locally, a fault-related cooling effect can be differentiated. This is more obvious around the s-Fs fault and its surroundings, shown in Fig. 3. These discrete cooling phenomena have pointed out the dynamic thermal behavior influenced by the fault structures and have also underlined that they may change heat transfer processes of the system.

Notably, the much higher temperatures in the left part of the model, well above 80 °C, compared to the average of 37–47 °C elsewhere, indicate significant local geological and hydrodynamic factors (Fig. 3). The high density of deep-penetrating faults in this area likely enhances its ability to accommodate the upward migration of warmer fluids from deeper strata, functioning as effective conduits for heat transfer. Moreover, abrupt bathymetric seafloor variations could produce variations in fluid circulation within subsurface flow conditions, potentially concentrating heat in focal positions. Additionally, the lower porosity of the gas hydrate-bearing layer relative to the surrounding sediments may also contribute to this temperature anomaly by reducing the layer's capacity to dissipate heat, further amplifying localized thermal effects.

In Fig. 3, around the s-FS fault the fluid velocity vectors demonstrate the presence of diffuse flow with extremely low fluid velocities, reaching as low as 1e-11 m/s, along the seismic section. This observation is further corroborated by the chirp data, which reported the existence of fluid vents. Notably, focused fluid flow velocities increase around and within the faults. Among these faults, fluid velocities can reach up to 9e-11 m/s (Fig. 3 a and b). This increase is attributed not only to the fault's effectiveness in transmitting fluid but also to the influence of the sea floor bathymetry. It further can be observed that the average fluid velocities of the gas hydrate layer and its temperature are both to be low at the right side of this model. Average velocities around 1e-11 m/s, the average temperature is about 30 °C (Fig. 3c).

The integration of seafloor bathymetry into our models has resulted in significant changes of the fluid inlet/outlet velocities, mainly due to seawater pressure variations along the seafloor, shown in Fig. 3. Fig. 3b highlights a large change in seafloor depth of approximately 600 m associated with the s-FS fault. This geological fault causes a high variation in pressure over short distances and thus affects fluid inlet/outlet velocities. Localized fluid velocities were increased over structures associated with steep, focused changes in seafloor bathymetry and corresponding underlying faulting. The focused fluid flow phenomena also resemble the situation at Vestnesa Ridge, as observed by Bünz et al. (2012).

Model 2 also presents temperatures over the left side well above 60 °C versus the rest, which stayed within the average of 20–30 °C, further emphasizing the influence of geological and hydrodynamic factors. Such high fault density and abrupt variations in seafloor bathymetry probably enhance focused heat transfer, while lower porosity in the gas hydrate layer reduces heat dissipation and amplifies local heating. Nevertheless, the general temperatures of the gas hydrate layer in Model 2 are below those of Model 1.

While diffuse flow along the seismic section appears with low velocities (~1e-11 m/s), focused flow velocities increase up to 9–10 m/s around faults (Fig. 4a and b). These variations are resulting from the activity of faults and seafloor bathymetry. On the right side of the model, the gas hydrate layer shows low averaged fluid velocities (~1e-11 m/s) and temperatures (~20 °C, Fig. 4c).

Whereas Models 3 and 4 clearly show that heat transfer is reduced by both an increased porosity of the gas-bearing sediment, as well as one closer to that of the surrounding sediments, Figs. 5 and 6 indicate that the temperature peak

inside the gas-bearing sediment on the left-hand side is as high as about 40 °C, and reduces to 25 °C towards the right side of the model. With higher values of porosity, the temperature distribution within the layer becomes more homogeneous, hence diminishing the possibility of local heating that may initiate gas hydrate dissociation.

This result underlines the importance of porosity—particularly under extremely low-porosity conditions—for smoothing heat transfer and thermal gradients within hydrate-bearing sediments. Extremely low porosity, as represented in the lowest values of our models and often adopted in previous studies, can give rise to focused thermal effects likely to destabilize gas hydrates. On the contrary, higher values disperse heat without any such risk. These findings offer insight into the thermal stability of gas hydrates in different geological environments and emphasize the need to understand sediment properties—especially in extreme low-porosity regimes—more thoroughly in order to predict hydrate behavior.The average temperatures for each computational cell within the layer defined as gas hydrate on the seismic section were calculated, and each point was plotted based on its corresponding temperature. This computation was done along the regions that are at the right and left corners of the model, and the areas where the calculations are performed are marked with red squares in the previous figures (Figs. 3–6). This was calculated for each model individually and plotted as such (Figs. 7 and 8). In order to further illustrate temperature profiles in Models 1–4, as influenced by porosity, a further simplification into two separate graphs (porosity and temperature) was effected for each model on behalf of the left and right regions of the model domain. In

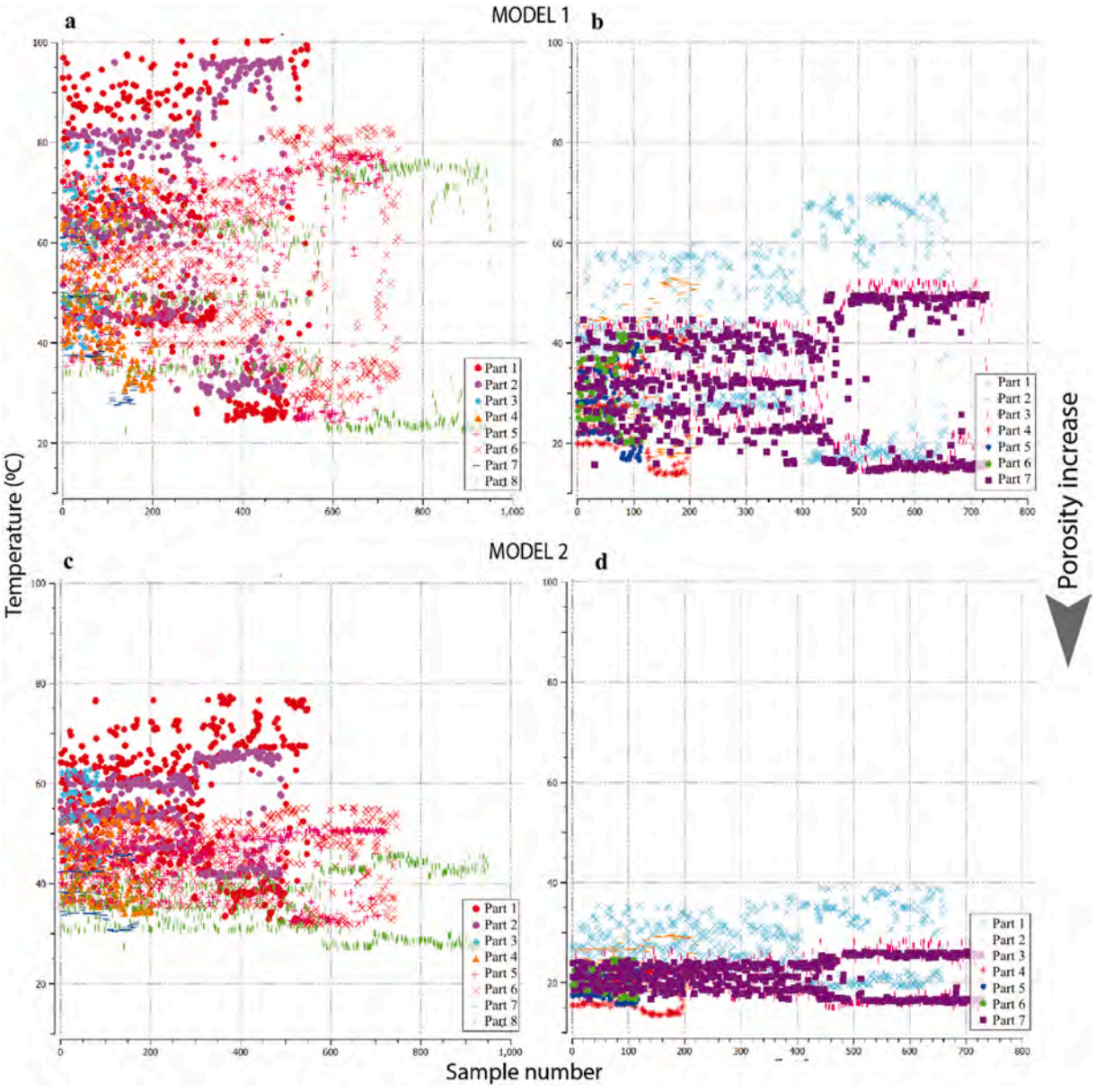

Fig. 7. The average temperature of each computational cell is plotted for Model 1 and 2. Panels **a** and **b** show the temperature values for the left and right sections of the Model 1, respectively. Panels **c** and **d** show the temperature values for the left and right sections of the Model 2, respectively. The values displayed were calculated within the regions enclosed by the red squares marked in the previous figures.

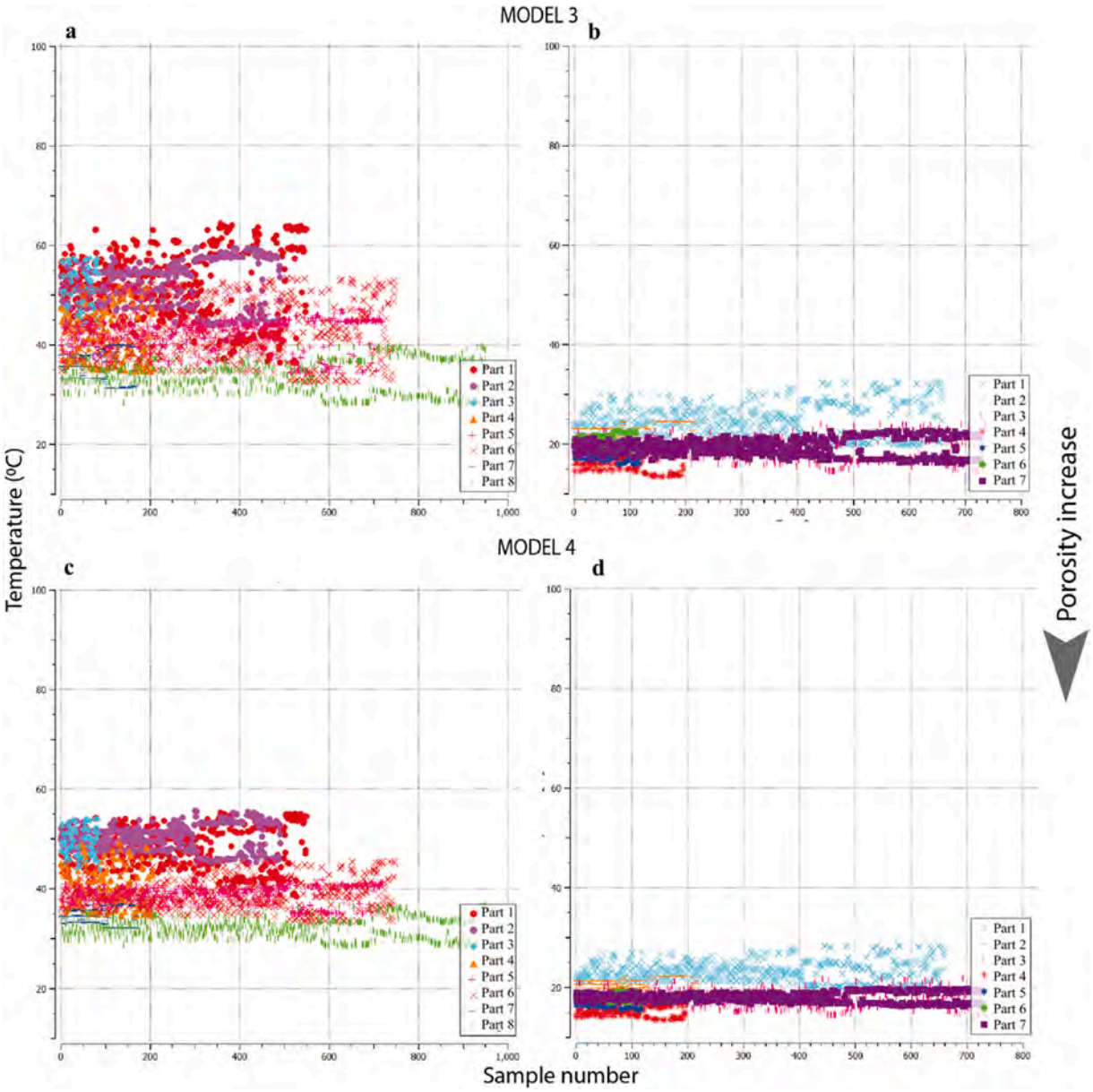

Fig. 8. The average temperature of each computational cell is plotted for Model 3 and 4. Panels **a** and **b** show the temperature values for the left and right sections of the Model 3, respectively. Panels **c** and **d** show the temperature values for the left and right sections of the Model 4, respectively. The values displayed were calculated within the regions enclosed by the red squares marked in the previous figures.

Model 1, showing the least porosity, on the left side, the temperature ranges from 20 to 100 °C, and on the right side from 10 to 70 °C. With increasing porosity across the models, a decrease in temperature values and homogenization is observed (Figs. 7 and 8). For example, Model 2 has temperatures between 30 °C and 80 °C on the left and between 10 °C and 40 °C on the right. Model 3 narrows the range further to between 30 °C and 65 °C and between 10 °C and 35 °C, respectively, while Model 4 has temperatures between 30 °C and 55 °C on the left and between 10 °C and 30 °C on the right. Moreover, particularly in the left zone of the model, with a better heat transfer factor, temperatures are scattered more than for the right one. This phenomenon is significantly more pronounced in models with lower porosity. For instance, this can be observed by comparing Fig. 7a (porosity 0.01) and Fig. 8c (porosity 0.2).

These temperature differences between the models suggest that hydrate-bearing sediments with low porosity may form localized thermal anomalies that are important for hydrate stability. Also, temperature transport is greater in the s-FS faulted regions of each model compared with other faulted model regions. The enhancement is both a result of greater depth of the s-FS faults and an additive effect from bathymetry-induced water pressures.

Combinational effects of variations in porosity, presence of faults and bathymetry can lead to the emplacement of thermal anomalies locally, further increasing the entrapment

of heat and enhancing temperature anomalies within the sediment. These temperatures have significant implications for the stability of gas hydrates, since hydrates are very sensitive to thermal and pressure variations. Such anomalies may only locally cause hydrate destabilization and methane release, and thus further detailed geological modeling is required to raise the degree of understanding and predictability of these dynamics for fault-dominated and tectonically active regions.

3. Conclusions

For the first time, numerical fluid flow models were applied in the current research to study gas hydrate dynamics in the Antarctic Peninsula's South Shetland Islands—a natural laboratory characterized by simplified geology and elevated environmental sensitivity. We built a high-resolution marine subsurface model and performed fluid flow simulations with seismic data in ANSYS Fluent, with significant geological inputs such as sediment thickness, fracture and fault networks, and water column thickness.

We applied a uniform set of thermal and physical rock properties for each rock unit, and a mesh discretization by triangular elements. Four numerical models with porosity values of 0.01, 0.05, 0.1, and 0.2—representing low-porosity conditions for hydrate-bearing sediments, with the lowest values reflecting extreme cases—were constructed to explore their impacts.

The findings emphasize the critical role of porosity, particularly under extremely low-porosity conditions, in determining heat transfer and thermal gradients within the sediments. Extremely low porosity values, typical in earlier models, can lead to localized thermal impacts that present a risk of destabilizing gas hydrates, whereas increased porosity allows more uniform dissipation of heat and reduces this risk. Such findings highlight the importance of adequately characterizing sediment properties—especially in extreme low-porosity regimes—in order to improve predictions of hydrate stability.

Furthermore, our simulations demonstrated that the combined effect of porosity heterogeneity, fault geometry, and seafloor bathymetry can produce localized thermal anomalies. These anomalies can entrap heat in sediments, thereby increasing local temperatures and inducing hydrate destabilization and methane release. Since hydrates are sensitive to pressure and temperature variations, these findings highlight the importance of incorporating detailed geological structure into models to reproduce the complex interactions governing hydrate systems.

In general, this work provides valuable insights into the geophysical and hydrodynamic controls on gas hydrate stability in environmentally sensitive and tectonically active regions. Model improvement in terms of geological models and spatial heterogeneity should be focused on in future studies to maximize predictive ability for hydrate behaviour under a variety of geological and environmental conditions.

CRediT authorship contribution statement

Doğa Düşünür Doğan: Writing – original draft, Visualization, Validation, Software, Methodology, Formal analysis, Conceptualization. **Selvican Türkdoğan:** Writing – review & editing, Software. **Neslihan Ocakoğlu:** Writing – review & editing, Software, Resources, Project administration, Data curation. **Umberta Tinivella:** Writing – review & editing, Software, Project administration, Data curation. **Michela Giustiniani:** Writing – original draft, Software, Project administration, Data curation. **Zehra Altan:** Writing – review & editing, Visualization. **Sinan Arık:** Writing – review & editing, Visualization.

Data availability

The data sets used and/or analysed during the current study available from the corresponding author on reasonable request.

Declaration of competing interest

The authors declare that they have no known competing financial interests or personal relationships that could have appeared to influence the work reported in this paper.

Acknowledgements

This study was supported by Memorandum of Understanding between Istanbul Technical University (ITU) and Department of Geophysical Engineering and Istituto Nazionale di Oceanografia e Geofisica Sperimentale (OGS) for the years 2018–2023. The geophysical data were acquired in 1989–2004 in the frame of the project “Gas Hydrates: impact on climate environmental of the sub-Antarctic regions (BSR)” supported by the Italian National Antarctic Program (PNRA). We also gratefully acknowledge the AspenTech Software Grant for Istanbul Technical University which enabled seismic data analysis with their software package Echos™ (https://www.aspentech.com/en/products/sse/aspen-echos). Bathymetry maps were created under ArcGIS software, freely available. Manuscript is dedicated to the memory of Serkan Üner.

References

Aharonov, E., Rothman, D.H., Thompson, A.H., 1997. Transport properties and diagenesis in sedimentary rocks: the role of micro-scale geometry. Geology 25, 547–550.

ANSYS, 2018. ANSYS fluent benchmark. Retrieved 21-06- 2018, from. https://www.ansys.com/solutions/solutions-by-role/it-professionals/platform-support/benchmarks-overview/ansys-fluent-benchmarks.

Barker, P.F., 1982. The Cenozoic history of the Pacific margin of the antarctic peninsula: ridge crest–trench interaction. J. Geolog. Soc. 139, 787–801. London.

Barker, P.F., Dalziel, I.W.D., 1983. Progress in geodynamics of the scotia arc region. In: Cabre, R. (Ed.), Geodynamics of the Eastern Pacific Region, Caribbean and Scotia Arcs, Geodyn. Ser., vol. 9. American Geophysical Union, Washington DC, pp. 137–170.

Bense, V., Person, M., 2006. Faults as conduit-barrier system to fluid flow in silicilastic sedimentary aquifers. Water Resour. Res. 42 (5). https://doi.org/10.1029/2005WR004480.

Bethke, C.M., Reed, J.D., Oltz, D.F., 1991. Long-range petroleum migration in the Illinois basin. AAPG Bull. 75 (5), 925–945. https://doi.org/10.1306/0C9B2899-1710-11D7-8645000102C1865D.

Bünz, S., Polyanov, S., Vadakkepuliyambatta, S., Consolaro, C., Mienert, J., 2012. Active gas venting through hydrate-bearing sediments on the vestnesa ridge, offshore W-Svalbard. Mar. Geol. 332–334, 189–197.

Dietrich, R., Rülke, A., Ihde, J., Lindner, K., Miller, H., Niemeier, W., Seeber, G., 2004. Plate kinematics and deformation status of the antarctic peninsula based on GPS. Global Planet. Change 42 (1–4), 313–321. https://doi.org/10.1016/j.gloplacha.2003.12.003.

Durham, W.B., Kirby, S.H., Stern, L.A., Zhang, W., 2003. The strength and rheology of methane clathrate hydrate. J. Geophys. Res. 108 (B4), 2182. https://doi.org/10.1029/2002JB001872.

Düşünür-Doğan, D., 2023. A study on the effects of fault architecture on fluid circulation in the Gediz Graben by the finite volume method. Solid Earth Sci. 8 (2), 146–159.

Düşünür-Doğan, D., Üner, S., 2019. Numerical simulation of groundwater flow and temperature distribution in aegean Coast of Turkey. J. Earth Syst. Sci. 128. https://doi.org/10.1007/s12040-019-1183-9.

Dziak, R.P., Bohnenstiehl, D.R., Stafford, K.M., et al., 2015. Source and levels of ambient ocean sound near the antarctic. PLoS One 10 (4), e0123425.

Ecker, C., Dvorkin, J., Nur, A., 1998. Sediments with gas hydrates: internal structure from seismic AVO. Geophysics 63, 1659–1669.

Fairley, J.P., Hinds, J.J., 2004. Field observation of fluid circulation patterns in a normal fault system. Geophys. Res. Lett. 31, L19502. https://doi.org/10.1029/2004GL020812.

Fontaine, F.J., Wilcock, W.S.D., 2007. Two-dimensional numerical models of open-top hydrothermal convection at high rayleigh and nusselt number: implications for mid-ocean ridge hydrothermal circulation. G-cubed 8 (7), 1–17.

Heffner, J., Fairley, J.P., 2006. Using surface characteristics to infer the permeability structure of an active fault zone. J. Sedim. Geol. 184, 255–265.

Helgerud, M.B., Dvorkin, J., Nur, A., Sakai, A., Collett, T., 1999. Elastic-wave velocity in marine sediments with gas hydrates: effective medium modeling. Geophys. Res. Lett. 26, 2021–2024.

Holmes, D., Connel, S., 1989. Solution of the 2D navier-stokes equations on unstructured adaptive grids. 9th Computational Fluid Dynamics Conference. American Institute of Aeronautics and Astronautics.

Hyndman, R.D., Davis, E.E., 1992. A mechanism for the formation of methane hydrate and seafloor bottom-simulating reflectors by vertical fluid expulsion. J. Geophys. Res. 97, 7025–7041.

Jin, Y., Lee, M., Kim, Y., Nam, S., Kim, K., 2003. Gas hydrate volume estimations on the south shetland Continental margin, antarctic peninsula. Antarct. Sci. 15 (2), 271–282.

Kim, Y., Kim, H.-S., Larter, R.D., Camerlenghi, A., Gambôa, L.A.P., Rudowski, S., et al., 1995. Tectonic deformation in the upper crust and sediments at the south shetland trench. Antarct. Res. Ser. 68. Cooper, American Geophysical Union, Washington, DC.

Kvenvolden, K.A., 1988. Methane hydratea major reservoir of carbon in the shallow geosphere? Chem. Geol. 71, 41–51.

Kvenvolden, K.A., 2002. Methane hydrate in the global organic carbon cycle. Terra Nova 14, 302–306.

Larter, R.D., Barker, P.F., 1991. Effects of ridge crest-trench interaction on antarctic-phoenix spreading: forces on a young subducting plate. J. Geophys. Res. 96 (B12), 19,583–19,607.

Lee, M.W., 2000. Gas hydrates amount estimated from acoustic logs at the Blake Ridge, Sites 994, 995, and 997. Proc. Ocean Drill. Progr. Sci. Results 164, 193–198.

Lodolo, E., Camerlenghi, A., Madrussani, G., Tinivella, U., Rossi, G., 2002. Assessment of gas hydrate and free gas distribution on the South Shetland margin (Antarctica) based on multichannel seismic reflection data. Geophys. J. Int. 148 (1), 103–119.

Loreto, M.F., Tinivella, U., 2012. Gas hydrate versus geological features: the South Shetland case study. Mar. Petrol. Geol. 36 (1), 164–171. https://doi.org/10.1016/j.marpetgeo.2012.04.005.

Loreto, M.F., Tinivella, U., Accaino, F., Giustiniani, M., 2011. Offshore Antactica Peninsula gas hyrate reservoir characterization by geophysical data analysis. Energies 4, 39–56.

Loreto, M.F., Düşünür-Doğan, D., Üner, S., İşcan-Alp, Y., Ocakoğlu, N., Cocchi, L., Muccini, F., Ligi, M., 2019. Fault-controlled deep hydrothermal flow in a back-arc tectonic setting, SE Tyrrhenian Sea. Sci. Rep. 9 (1). https://doi.org/10.1038/s41598-019-53696-z.

Neagu, R.C., Tinivella, U., Volpi, V., Rebesco, M., Camerlenghi, A., 2009. Estimation of biogenic silica contents in marine sediments using seismic and well log data: sediment Drift 7, Antarctica. Int. J. Earth Sci. 98, 839–848.

Nimblett, J., Ruppel, C., 2003. Permeability evolution during the formation of gas hydrates in marine sediments. J. Geophys. Res. 108 (B9), 2420. https://doi.org/10.1029/2001JB001650.

Patankar, S., 1980. Numerical Heat Transfer and Fluid Flow. CRC Press, New York.

Paull, C.K., Matsumoto, R., Wallace, P.J., 1996. Leg 164 Science Party. In: Proceedings of the Ocean Drilling Program, Initial Reports, vol. 164. Ocean Drill. Program, College Station, Tex.

Şen, E., Doğan, D., 2021. Finite volumemodeling of bathymetry and fault-control ed fluid circulation in the Sea ofMarmara. Turk. J. Earth Sci. 1 (1), 1–20.

Solovyov, V.D., Bakhmutov, V.G., Korchagin, I.N., Levashov, S.P., Yakymchuk, N.A., Bozhezha, D.N., 2011. Gas hydrates accumulations on the South Shetland continental margin: new detection possibilities. J. Geol. Res. https://doi.org/10.1155/2011/514082.

Song, Y., Kuang, Y., Fan, Z., Zhao, Y., Zhao, J., 2018. Influence of core scale permeability on gas production from methane hydrate by thermal stimulation. Int. J. Heat Mass Tran. 121, 207–214.

Tinivella, U., 1999. A method for estimating gas hydrate and free gas concentration in marine sediments. Boll. Geofis. Teor. Appl. 40 (1), 19–30.

Tinivella, U., 2002. The seismic responce to overpressure versus gas hydrate and free gas concentration. J. Seismic Explor. 11 (3), 283–305.

Tinivella, U., Accaino, F., 2000. Compressional velocity structure and Poisson's ratio in marine sediments with gas hydrate and free gas by inversion of reflected and refracted seismic data (South Shetland Islands, Antarctica). Mar. Geol. 164 (1–2), 13–27.

Tinivella, U., Lodolo, E., Camerlenghi, A., Boehm, G., 1998. Seismic tomography study of a bottom simulating reflector off the South Shetland Islands (Antarctica). Geol. Soc. Lond. Special Publ. 137, 141–151.

Tinivella, U., Accaino, F., Camerlenghi, A., 2002. Gas hydrate and free gas distribution from inversion of seismic data on the South Shetland Margin (Antarctica). Mar. Geophys. Res. 23, 109–123.

Tinivella, U., Accaino, F., Vedova, B.D., 2008. Gas hydrates and active mud volcanism on the South Shetland continental margin, Antarctic Peninsula. Geo Mar. Lett. (2), 97.

Tinivella, U., Loreto, M.F., Accaino, F., 2009. Regional Versus Detailed Velocity Analysis to Quantify Hydrate and Free Gas in Marine Sediments: the South Shetland Margin Case Study, vol 319. The Geological Society, London, pp. 103–119. Special Publications.

Üner, S., Dogan, D.D., 2021. An integrated geophysical, hydrological, thermal approach to finite volume modelling of fault-controlled geothermal fluid circulation in Gediz Graben. Geothermics 90. https://doi.org/10.1016/j.geothermics.2020.102004.

Vargas-Cordero, I., Giustiniani, M., Tinivella, U., Villar-Munoz, L., Alessandrinş, G., 2021. Gas hydrate System offshore Chile. Energies 14 (3), 709. https://doi.org/10.3390/en14030709.

Zaldívar, J.G., Maestro, A., Martinez, J.L., Galdean, C.S., 2006. Elephant Island recent tectonics in the framework of the scotia-antarctic-south shetland block triple junction (NE antarctic peninsula). In: Fütterer, D. K., Damaske, D., Kleinschmidt, G., Miller, H., Tessensohn, F. (Eds.), Antarctica: Contributions to Global Earth Sciences. Springer-Verlag, Berlin Heidelberg New York, pp. 271–276, 2006.